Covert information sharing via ghost displacement

U. Zanforlin,[1,*] G. Tatsi,[2] J. Jeffers,[2] and G. S. Buller[1]

[1]*Scottish Universities Physics Alliance, Institute of Photonics and Quantum Sciences, School of Engineering and Physical Sciences, Heriot-Watt University, David Brewster Building, Edinburgh EH14 4AS, Scotland, United Kingdom*

[2]*Scottish Universities Physics Alliance, Department of Physics, University of Strathclyde, John Anderson Building, 107 Rottenrow, Glasgow G4 0NG, Scotland, United Kingdom*

(Received 6 May 2022; accepted 3 January 2023; published 24 February 2023)

Ghost imaging research has demonstrated that it is possible to reproduce an image of an object that has not interacted with the imaging light. In this paper we describe theoretically and demonstrate experimentally a coherent displacement imposed nonlocally on one mode of a two-mode state, replicating the ghost imaging effect in the coherent-state basis. We use it to show the possibility of a form of covert information sharing via a *ghost displacement* operation which enables two distant users to retrieve amplitude and phase information modulated onto a phase-independent thermal state, based only on correlated detection statistics. The displacement operation also provides a secondary probabilistic amplification effect on the mean photon number of the displaced thermal state, which could be exploited for covert quantum illumination experiments.

DOI: 10.1103/PhysRevA.107.022619

I. INTRODUCTION

Optical physicists associate the word *ghost* with the observation of an object that has not interacted with its measuring system, most notably in ghost imaging where the object is generally not in the path of light reaching the measurement camera [1–4]. The first demonstration of such an imaging technique made use of entangled sources, leveraging their unique nonlocal quantum properties [5–7]. However, further studies showed that similar results could be obtained via thermal light [8–11] resulting in arguments about whether this effect should be considered quantum or classical in nature [12]. The effect comes about because thermal radiation displays a characteristic photon bunching distribution for which, at any time, photons are statistically more likely to be observed in *multiphoton clusters* rather than being randomly distributed as for radiation with Poissonian statistics [13–15]. The states of light that are used for ghost imaging are normally locally indistinguishable from weak thermal beams. Without knowledge of the measurement results at the detectors it is difficult for an external observer to determine that the imaging is taking place.

In the light of the above many researchers have started to question if the properties of thermal radiation could also be exploited in other fields, such as quantum state amplification and discrimination [16–21] as well as quantum communication [22,23]. In quantum communication, comprehensive work has been dedicated to establishing if current quantum key distribution (QKD) protocols could also be applied outside the scope of single-photon sources [24] or weak coherent states [25] while retaining the same level of information-theoretic security [26]. From this research a new branch of QKD protocols was born: continuous-variable QKD (CV-QKD) [27,28]. The main difference in CV-QKD systems is that the physical properties used to generate a secret key are no longer encoded in discrete quantities, e.g., discrete phase alphabets [29], polarization [30], or time [31], but in the continuous quadrature components of light, e.g., the $\hat{P}$ and $\hat{Q}$ field quadratures associated with the momentum and position variables $\hat{p}$ and $\hat{x}$ respectively [32]. Homodyne and heterodyne detection are commonly used to retrieve this quadrature information. The key feature of such schemes is that they are capable of retrieving quadrature information from the original modulated coherent signal, discarding the inherently noisy thermal background [33]. Recent work has also shown that similar results could also be obtained even if the original signal states are purely thermal [34–36]. However, none of the research undertaken in this field has shown interest in leveraging the "ghost" -like features of thermal radiation in the context of quantum information.

In this paper we bridge this gap by presenting a hybrid covert information sharing system employing thermal states and using a coherent *ghost displacement* (GD) operation. The displacement operation imprints both phase and intensity information on one output of a split thermal signal, which can later be retrieved from the output that has not interacted with the displacement state, in analogy with ghost imaging. Coherent displacement prior to detection of intermediate photon numbers (>20) has recently been studied, and shown to impart heralded non-Gaussianity on an initially squeezed Gaussian signal [37]. This information sharing is covert, but not necessarily information theoretically secure. To show such

*U.Zanforlin@hw.ac.uk

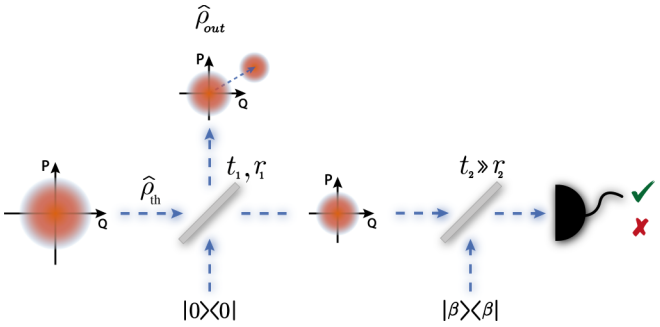

FIG. 1. Ghost displacement mechanism. Half of the original thermal state $\hat{\rho}_{\rm th}$ is displaced at a highly transmissive BS ($t_2 \approx 1$) via mixing with a coherent state $|\beta\rangle\langle\beta|$. A SPAD monitors one output mode of BS_2 and when it does not fire, the output state $\hat{\rho}_{\rm out}$ is conditioned to a displaced thermal state of higher mean photon number.

security a detailed communication protocol would need to be specified as in QKD systems [38–40]. By covert we simply mean that the information sharing is hidden from an external party to some degree in the noise associated with thermal light. It has been shown that covert quantum communication is possible when such noise is present [41,42]. We discuss the covertness of our scheme in more detail in Sec. IV. Additionally, because of the nature of the displacement operation, our system also shows quantum amplification capabilities when the original thermal state is conditioned on specific photon detection statistics. Interestingly, the magnitude of the amplification effect is directly proportional to the amplitude of the displacement operation, chosen by the local encoder, a feature that could be exploited for covert quantum imaging experiments [43].

II. GHOST DISPLACEMENT

The measurement technique used for the GD operation is based on coherent-state displacement, a nonlocal quantum operation that conditionally changes both the mean photon number and phase of an output quantum state [21]. This measurement is performed on one output of a beam splitter (BS) that has been used to split thermal light. As we shall see, when successful, this measurement applies a displacement to the state in the other output arm of the beam splitter. This displacement is applied to the second beam despite there being no local interaction with a displacing coherent state—a ghost displacement. The thermal state $\hat{\rho}_{\rm th}$ with mean photon number $\bar{n}$ can also be expanded in the coherent-state basis in terms of its P function [44]:

$$\hat{\rho}_{\rm th} = \frac{1}{\pi\bar{n}} \int e^{-\frac{|\alpha|^2}{\bar{n}}} |\alpha\rangle\langle\alpha|\, d^2\alpha \tag{1}$$

where the integral is performed over the entire complex plane so that $d^2\alpha \equiv d\,\mathrm{Re}[\alpha] d\,\mathrm{Im}[\alpha]$. The combined input state to our device (Fig. 1) is a three-mode input state formed of the thermal state, the vacuum state, and a coherent state that forms the displacement which can be expressed as follows:

$$\hat{\rho}_{\rm in} = \frac{1}{\pi\bar{n}} \int e^{-\frac{|\alpha|^2}{\bar{n}}} |\alpha, 0, \beta\rangle\langle\alpha, 0, \beta|\, d^2\alpha \tag{2}$$

where α is the coherent-state basis used to define the thermal state, the null term indicates the vacuum state, and β parametrizes the displacement amplitude prior to the mixing beam splitter. Using the same notation adopted in Fig. 1, the joint output state of the three modes $\hat{\rho}_{\rm out}$, after undergoing two BS transformations, becomes

$$\hat{\rho}_{\rm out} = \frac{1}{\pi\bar{n}} \int e^{-\frac{|\alpha|^2}{\bar{n}}} |t_2 t_1\alpha - r_2\beta,\ r_1\alpha,\ t_2\beta + r_2 t_1\alpha\rangle\langle t_2 t_1\alpha - r_2\beta,\ r_1\alpha,\ t_2\beta + r_2 t_1\alpha|\, d^2\alpha \tag{3}$$

where t_i, r_i with $i = 1, 2$ are the transmittance and reflectance respectively of BS_1 and BS_2 of Fig. 1. We represent physical detection of the output state by tracing out the unmonitored mode and conditioning on a no-click event, so the resulting single-mode state takes the following form:

$$\hat{\rho}_{\rm out|\not\times} = \frac{1+\eta\bar{n}t_2^2t_1^2}{\pi\bar{n}r_1^2} \int \exp\left\{-\left(\frac{1+\eta\bar{n}t_2^2t_1^2}{\bar{n}r_1^2}\right) \times \left|\alpha - \frac{\eta\bar{n}t_2t_1r_2r_1\beta}{1+\eta\bar{n}t_2^2t_1^2}\right|^2\right\} |\alpha\rangle\langle\alpha|\, d^2\alpha \tag{4}$$

where η is the detection quantum efficiency. This state has the form of a thermal state of mean photon number

$$\overline{m} = \frac{\bar{n}r_1^2}{1+\eta\bar{n}t_2^2t_1^2} \tag{5}$$

displaced by a coherent amplitude

$$\gamma = \frac{\eta\bar{n}t_2t_1r_2r_1\beta}{1+\eta\bar{n}t_2^2t_1^2}. \tag{6}$$

The striking feature of Eq. (4) is that, despite the state $\hat{\rho}_{\rm out}$ not having interacted with $|\beta\rangle\langle\beta|$ (see Fig. 1), it still shows a correlation with the displacement operation.

This effect is at the heart of the GD mechanism which conditions the output state. In order to give an idea of the conditioning effect, the mean photon number of the output state, when the measurement is successful, $\bar{n}_{\not\times}$, is

$$\bar{n}_{\not\times} = \frac{\bar{n}r_1^2}{1+\eta\bar{n}t_2^2t_1^2} + \left|\frac{\eta\bar{n}t_2t_1r_2r_1\beta}{1+\eta\bar{n}t_2^2t_1^2}\right|^2. \tag{7}$$

The second term in Eq. (7) is proportional to the mean photon number of the coherent amplitude $|\beta|^2$, so theoretically the output mean photon number is *unlimited*, whatever the (nonzero) mean photon number of the original thermal state, $\bar{n}$, that is input into the device. The phase information from the coherent amplitude is also imprinted nonlocally on the output state, which could be exploited in a quantum communication framework for covert information sharing. Of course sometimes the detector fires and when it does, the output state is discarded. The effect of non-unit-detection efficiency η on our no-click measurement is to lower the effective amplitude of the coherent displacement $|\beta\rangle\langle\beta|$, decreasing the amplitude of the GD state [Eq. (6)] and at the same time increasing the thermal component slightly [Eq. (5)], both of which change the phase variance of the shared state but not its central value. The GD amplitude can easily be restored by increasing the value of β, so our scheme is robust to inefficiency (and dark counts are naturally excluded). The overall success probability

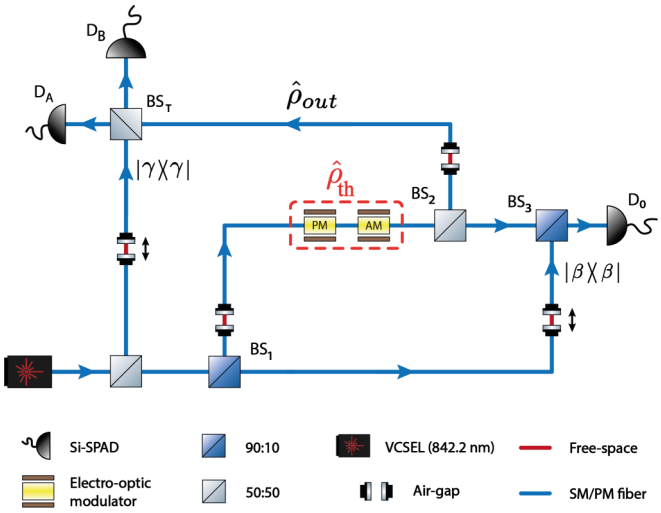

FIG. 2. Experimental setup of the ghost displacement operation. A VCSEL source (842.2 nm) produces a train of coherent pulses at 1-MHz repetition rate. Phase and amplitude modulators (PM and AM) modulate individual laser pulses to simulate a pseudothermal source. A 90:10 beam splitter (BS_3) performs the displacement operation between the newly generated thermal state and a residual coherent state $|\beta\rangle\langle\beta|$ that is unmodulated. A "copy" of the thermal state is sent to a tomography stage (BS_T) where a suitable reference signal $|\gamma\rangle\langle\gamma|$ is chosen to perform a full tomographic reconstruction of the state $\hat{\rho}_{\text{out}}$. Adjustable air gaps are placed in different optical paths of the interferometers in order to provide control over the phase stabilization of the system. All detectors are Si-SPADs whose signals are registered and processed by a TCSPC module (not shown) for postprocessing and correlation analysis.

of the protocol, P_S, associated with a no-click event is

$$P_S = \frac{1}{1+\eta\bar{n}t_2^2t_1^2}\exp\left\{-\frac{\eta r_2^2|\beta|^2}{1+\eta\bar{n}t_2^2t_1^2}\right\}, \tag{8}$$

which decays with increasing coherent amplitude $|\beta|^2$ and thermal state mean photon number $\bar{n}$. Non-unit-detection efficiency increases the success probability.

III. EXPERIMENTAL VERIFICATION

The experimental setup is shown in Fig. 2. A vertical cavity surface emitting laser (VCSEL) with a central wavelength of 842.2 nm and a 0.11-nm linewidth, operated in pulsed mode at a repetition rate of 1 MHz, produced a train of pulses coupled to a single mode polarization maintaining fiber. A variable optical attenuator (not shown) was used to adjust the mean photon number of the pulses to a level compatible with the sensitivity of commercial single-photon avalanche diodes (SPADs). A 90:10 BS routed part of the light to two electro-optic modulators which were used to produce the pseudothermal light (see Appendix C for more details) while the remaining unmodulated pulses were sent to the displacement stage. A 50:50 BS (BS_2) was used to split the newly generated thermal light into two copies of half the mean photon number: one reaching the displacement stage (BS_3) where it was mixed with the pulses corresponding to the coherent state $|\beta\rangle\langle\beta|$ and the other reaching the tomography stage where a reference signal $|\gamma\rangle\langle\gamma|$ was chosen to perform a full state reconstruction on the ghost-displaced thermal state. The optical setup was composed of two interferometers: one used for the displacement operation and one for state tomographic reconstruction. In order to achieve optimal spatial and temporal overlap between the attenuated laser pulses at the different BSs, adjustable air gaps were inserted in key optical paths which allowed us to adjust and maintain a constant phase reference so that optimal interference visibility could be reached throughout a full integration time. Multiplexed reference signals allowed us to tune each interferometer separately and independently reaching interferometric visibilities as high as 98% (see Appendix D for more details). The output modes of BS_3 and BS_T were monitored by silicon SPADs (Si-SPADs) with 40% detection efficiency at 850-nm wavelength connected to a time correlation single-photon counting (TCSPC) module that collected time tags information for postprocessing and correlation analysis with picosecond resolution. The entire setup was placed in a controlled environment to limit temperature fluctuations and mechanical vibrations.

The GD operation displaces an output thermal state according to Eq. (4), which indicates that the coherent contribution proportional to the state $|\beta\rangle\langle\beta|$ is phase dependent, i.e., according to the phase of β the thermal state is reduced in magnitude and mapped to a different position in the phasor diagram even if the mapped state has the same total mean photon number. In order to establish this phase-dependent correlation, the mean photon number of the reference light corresponding to $|\gamma\rangle\langle\gamma|$ reaching BS_T was chosen so that it could reroute the coherent contribution of Eq. (7) only to one of the two output modes, thus restoring half of the original thermal state to the other. Only half of the original thermal state can be retrieved because of the action of BS_T on the states $\hat{\rho}_{\text{out}}$ and $|\gamma\rangle\langle\gamma|$ (see Fig. 2). This procedure is effectively equivalent to an antidisplacement operation where half of the original thermal state is retrieved. Figure 3 shows the normalized count rates of both detector D_A and D_B as a function of the phase imprinted on $|\beta\rangle\langle\beta|$ when the reference phase of $|\gamma\rangle\langle\gamma|$ is kept constant for a displacement's mean photon number of $|\beta|^2 = 3.71 \pm 0.01$. The normalization is performed so that the maxima correspond to the configurations where the reference state maximizes the coherent contribution towards that specific detector and the minima correspond to the configurations where the state measured is purely thermal without any coherent displacement. In other words, the maxima coincide with the detection of a twofold displaced thermal state while the minima coincide with that of a pure thermal state. As expected, the two sinusoidal responses are out of phase by half a cycle, i.e., the total mean photon number must be conserved for all θ values. Each data point is the result of an average over 25 individual acquisitions of duration 1 s in order to reduce the Poissonian error associated with the measured detection statistics.

Despite the rather simple representation of Fig. 3 its implications are quite significant. The sinusoidal responses of the two detectors are only possible because $\hat{\rho}_{\text{out}}$ must possess some displacement characteristics that the reference state

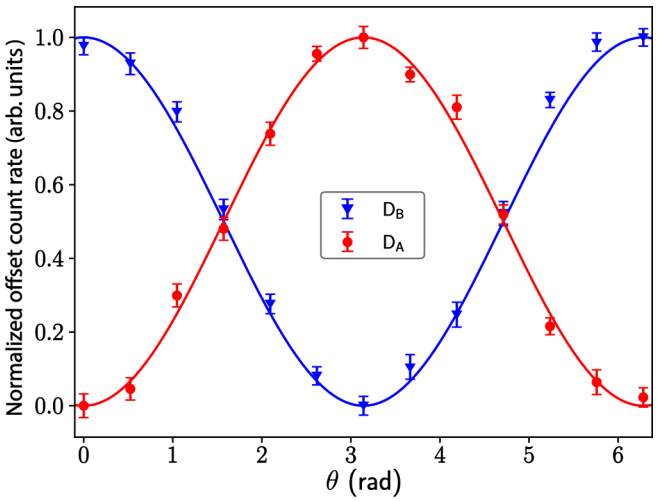

FIG. 3. Normalized offset count rates of the tomography detectors D_A and D_B as a function of the phase encoding θ of the displacement state $|\beta\rangle\langle\beta|$, conditioned on detector D_0 not firing. Colored data points depict experimental values while solid lines are fit interpolations. All error bars reflect standard errors computed over sets of 25 measurements each.

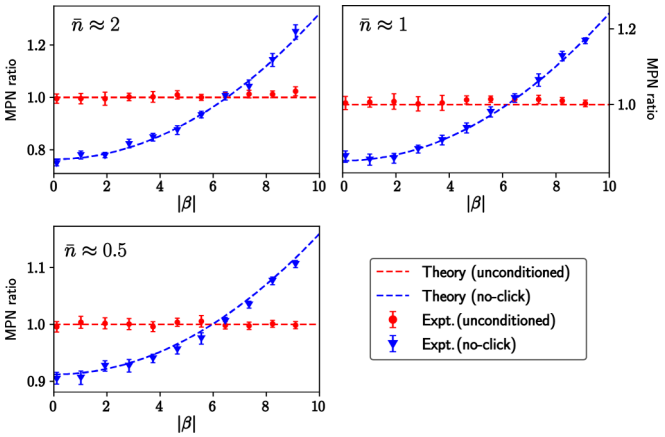

FIG. 4. Mean photon number ratios of the output state $\hat{\rho}_{\text{out}}$ as a function of the displacement's amplitude $|\beta|$. Blue triangles show the ratio of the mean photon number of the output state when conditioned on a no-click event from D_0 to that of the unconditioned case, i.e., $\bar{n}_{\text{✗}}/\langle n\rangle$, while red circles show the ratio of the experimental $\langle n\rangle$ to the expected theoretical value $\langle n\rangle_{\text{th}} = \bar{n}r_2^2$. Dashed colored lines represent the theoretical predictions of the model using the experimental values for the splitting ratios of BS_3, BS_2, and the detection efficiencies of D_0, D_A, and D_B. All errorbars reflect standard errors computed over sets of 25 measurements each.

$|\gamma\rangle\langle\gamma|$ is able to reroute to one specific detector. If this were not the case then, on average, detectors D_A and D_B would produce constant count rates irrespective of the phase imprinted on $|\beta\rangle\langle\beta|$ or of the state itself for that matter since it never reaches either detector. Due to this phase-dependent GD operation, a covert quantum information sharing system can be envisioned where these phase correlations could be exploited by two distant parties to generate correlated measurements similarly to conventional QKD systems [45]. If an eavesdropper were to intercept the output state $\hat{\rho}_{\text{out}}$ as it traveled towards the tomography stage, i.e., from BS_2 to BS_T, if they had no knowledge of the measurements, they would only detect a thermal state since the GD only takes place when the state is correlated with a click or no-click event from detector D_0, which is positioned after the output state is tapped off.

The sharing of information in amplitude and/or phase can be covert if the two parties, one monitoring D_0 and the other at the tomography stage, agree on the possible set of displacement amplitudes beforehand. If the eavesdropper does not have this information she cannot gain any meaningful information. The party monitoring D_0 would simply disclose a string that indicates when the detector did not fire, so that the other party could perform the appropriate measurement. The eavesdropper would simply detect a thermal state, tapped off before the GD, that can be adjusted to hide in the environmental thermal background for further covertness. Moreover, if the eavesdropper does not even know what type of measurements the two parties perform then the situation is more covert still.

Another important aspect of the GD is that the coherent displacement can always be observed for any amplitude $|\beta|$, therefore, it is possible to choose any suitable value that can satisfy specific security constraints of a quantum communication system. As indicated in Eqs. (4) and (7), the GD operation not only modifies the nature of the state but it also increases the corresponding mean photon number by an amount proportional to the displacement's amplitude $|\beta|$. Specifically, whenever the reference state $|\gamma\rangle\langle\gamma|$ minimizes the count rates of either D_A or D_B (the minima of Fig. 3), the subset of counts conditioned on a no-click event from D_0 corresponds to a state of higher mean photon number. Figures 4(a)–4(c) show the ratios of the computed mean photon numbers of the output state $\hat{\rho}_{\text{out}}$ for different conditioning criteria to the mean photon number of the unconditioned thermal state $\langle\hat{n}\rangle$ as a function of the displacement's amplitude $|\beta|$ for different $\bar{n}$. As expected, the ratio for the unconditioned thermal state is constant across the entire $|\beta|$ range while the one relative to the state conditioned on a no-click event is monotonically increasing as indicated by Eq. (7). Similarly to the previous analysis, the data points shown are the result of 25 individual acquisitions of 1 s each. For the range $|\beta| > 4$, additional attenuation (not shown in Fig. 2) was added to the output mode of BS_3 to prevent D_0 from saturating due to the high mean photon numbers of the associated displacement states. The results of Fig. 4 confirm once more that when no conditioning criteria are applied to the output state, the associated average mean photon number $\langle\bar{n}\rangle = \bar{n}\, r_2^2$ simply depicts a pure thermal state while the GD mechanism effectively displaces the state so that its associated mean photon number is "amplified" by an amount proportional to the displacement's amplitude $|\beta|$. This amplification effect is covert to any party that does not know the detection result at D_0. They would simply see thermal light, whose mean photon number could be matched to the background. Given that the intensity of the ghost displaced state is effectively unlimited, the effect could be exploited for quantum covert illumination experiments [7] where LIDAR-like measurements [46,47] could be enabled only when the mean photon number of the input signal is above a specific security threshold.

IV. DISCUSSION

In this paper we have presented a displacement technique that we have dubbed *ghost displacement*, in which phase and intensity modulations are shared between two nonlocal thermal states via beam splitter transformations. This mechanism is possible because of the strong correlations present in thermal states that are partially split between the outputs of a beam splitter. The experimental results confirmed that the GD operation is phase sensitive thus envisioning its use within the context of quantum communications where two distant parties could extract such information to generate correlated measurements similarly to conventional QKD systems [45].

Differently from quantum teleportation, the nonlocal behavior of GD stems from the use of a two-mode "classically" correlated state which is measured in a particular basis, i.e., coherent-state basis. Moreover, teleportation is a feature commonly attributed to highly nonclassical states, such as entangled states, which share stronger measurement-induced correlations than any classical state. These correlations are usually measured via Bell state measurements [48,49]. Here, instead, we use semiclassical states where measurement-induce correlations emerge from the photon bunching nature of thermal states.

Our findings also show that the GD effect is observable over a wide range of amplitudes of the displacement state thus allowing the users to choose the optimal mean photon number compatible with the security constraint of the desired quantum protocol [50]. The paper presented here does not describe the implementation and description of a QKD protocol nor the accompanying security analysis. Nor does the described GD operation imply information theoretical security for the hypothetical communication system. The underlying physical process can only provide covertness similarly to ghost imaging systems. In other words, the envisioned communication exchange should be viewed as a quantum oblivious technique used to share phase and intensity information nonlocally between two users. We speculate, however, that a modified version of thermal-based QKD-like protocols [34–36] might be employed as recent works have demonstrated security proofs for CV-QKD protocols [38–40]. However, a comprehensive analysis, simulation, and implementation of a carefully selected and designed protocol would be required to ensure its applicability and compatibility with our system.

An obvious question arises as to the degree of covertness that we can obtain. This depends on the prior knowledge of the external party. If they do not know that we are trying to exchange information they can realistically only detect that we are sending light with thermal statistics. We can hide even this if our mean photon number is identical to the background. If the external party does suspect that we are exchanging information they cannot easily tell how. The type of measurement that we perform is also hidden from them.

Additionally to the phase-transfer experimental results, we also showed the secondary effect of the GD operation where the mean photon number of the ghost-displaced thermal state is either amplified or attenuated probabilistically according to the amplitude of the displacement operation when the output state is conditioned on a click or no-click event from a monitoring detector. Conditional amplification or attenuation is a well-known feature of general photon subtraction schemes with pure thermal states [21,51–55] where the probabilistic operation relies on the nature of the quantum states rather than the action of nonlinear optical phenomena [56–58]. We have shown here that it is also a feature of GD and could be exploited for quantum covert illumination experiments [7] where time-of-flight imaging setups would be allowed to reconstruct three-dimensional images of an object only when the mean photon number of the input states satisfies a specific thresholding constraint.

All relevant data are available from the Heriot-Watt University data archive [59].

ACKNOWLEDGMENTS

This work was supported by the Engineering and Physical Sciences Research Council through Quantum Communications Hub Grants No. EP/T001011/1 and No. EP/N003446/1, QuantIC Grant No. EP/T00097X/1, and SPEXS Grant No. EP/S026428/1.

APPENDIX A: THERMAL STATES

Thermal radiation is normally associated with the spectral emission of a blackbody at a constant temperature [60]. In the quantum framework a single thermally excited mode of the optical field can be fully described by the density operator $\hat{\rho}_{\rm th}$:

$$\hat{\rho}_{\rm th} = \sum_{n=0}^{\infty} P_n |n\rangle\langle n| \tag{A1}$$

where $|n\rangle\langle n|$ is the projector on the Fock states $|n\rangle$, $\bar{n}$ is the mean photon number, and $P_n = \frac{\bar{n}^n}{(1+\bar{n})^{1+n}}$ is the probability of finding n photons in the mode [61]. One feature of this probability distribution is that its variance is bigger than its mean which is typical of a super-Poissonian distribution [62]. A direct consequence of this is that thermal states show strongly correlated intensity fluctuations indicative of photon bunching effects, i.e., the probability of finding a photon a time τ before or after another one is not uniformly distributed [13]. This effect was first discovered by Hanbury Brown and Twiss (HBT) who used it to measure the angular size of distant stars [63]. In their work, HBT measured the second order correlation function $g^{(2)}(\tau)$ with two spatially separated detectors and found that at $\tau = 0$ the number of correlations was twice that at long delays, i.e., $\tau \to \pm\infty$. This phenomenon is now understood in terms of quantum interference and joint detection probability [64]. The function $g^{(2)}(\tau)$ is defined quantum mechanically for a single mode state with constant mean photon number in terms of the density operator $\hat{\rho}$ and the annihilation and creation operators $\hat{a}$ and $\hat{a}^\dagger$ at time t and delayed time τ respectively:

$$g^{(2)}(\tau) = \frac{\mathrm{Tr}[\hat{\rho}\,\hat{a}(t)^\dagger \hat{a}(t+\tau)^\dagger\,\hat{a}(t)\hat{a}(t+\tau)]}{\{\mathrm{Tr}[\hat{\rho}\,\hat{a}^\dagger(t)\,\hat{a}(t)]\}^2}. \tag{A2}$$

This function tends to 1 for large τ and for classical radiation one always has $g^{(2)}(0) \geqslant g^{(2)}(\tau)$, with $g^{(2)}(0) = 2$ for thermal radiation [65]. This high degree of coherence at zero temporal delay effectively means that if we detect a photon in a

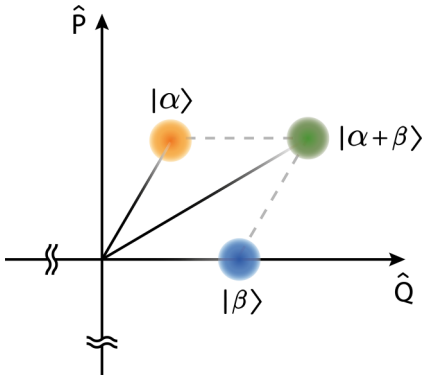

FIG. 5. coherent-state displacement representation. A coherent state $|\beta\rangle$ is displaced by the state $|\alpha\rangle$ and mapped to a new coherent state with a mean photon number of $|\alpha+\beta|^2$ and a phase of arctan $(\frac{\mathrm{Im}[\alpha+\beta]}{\mathrm{Re}[\alpha+\beta]})$. The operation preserves the noise profile of the original states due to the unitary nature of the operator.

thermal beam at a particular time it is twice as likely that we detect another at the same time, compared to detecting another at a time after a long delay. It is this effect that underlies ghost imaging, in which typically the light from a thermal state is divided in two by a beam splitter. When a detector in one of the outputs fires, this conditions the other output to have a higher photon number [21]. If the state has multiple spatial modes and if an object is placed in the first arm, a detection here forces the intensity image of the object to be imprinted on the light in the other arm (that has not interacted with the object), hence ghost imaging. The strong correlations inherent in thermal states are not only limited to the photon number basis. In ghost imaging the click measurement is a number basis measurement, but we can access different correlations by performing a different measurement. In this paper we describe and report the effect of measurements in the coherent-state basis.

APPENDIX B: COHERENT-STATE MEASUREMENT

Coherent displacement is a unitary quantum operation that maps one coherent state to another [66]. Its mathematical representation is that of a unitary operator $\hat{D}(\alpha)$ which acts on a coherent state $|\beta\rangle$ as follows:

$$\hat{D}(\alpha)|\beta\rangle = |\alpha+\beta\rangle \tag{B1}$$

where both α and β are complex numbers. Displacement-type operations are used in coherent-state discrimination experiments via BS transformations [67] (see Fig. 5).

In our paper, we use a physical operation that produces the theoretical displacement in the appropriate limit to measure an unknown state in a coherent-state basis (see Fig. 1). The operation is based on mixing the state to be measured with a coherent state of amplitude β at a highly transmitting $t \to 1$ beam splitter. The transmitted state is detected with a Geiger-mode detector (the reflected part is ignored) and, when this detector does not fire, the combination of state mixing and detector result corresponds to a measurement in the state $|-r\beta\rangle$. There are a few points to make about the measurement. First, the reflection coefficient is small (typically $<1\%$), and is effectively made smaller by any non-unity-detector efficiency. This can be easily compensated for by increasing the amplitude β. Secondly, by conditioning on a no-click event, the measurement should be insensitive to detector dark counts as they will be automatically excluded.

APPENDIX C: PSEUDOTHERMAL STATE GENERATION

Thermal states are states of well-defined mean photon number but undefined phase [62]. The thermal nature of these quantum (classical) states of light is usually described as an incoherent collection of spatial and/or temporal modes that reduces their associated coherence length and time [60]. Common optical sources that produce thermal radiation are LEDs [68] or coherent sources that interact with coarse semitransparent surfaces [69]. However, these sources do not retain a relative phase reference which could be used for further interferometric measurements. In our case, a common relative phase was necessary between the displacing amplitude and the tomography reference signal $|\gamma\rangle\langle\gamma|$ in order to properly reconstruct the state $\hat{\rho}_{\mathrm{out}}$. Therefore, a different approach was needed to generate the required thermal state. Due to the semiclassical nature of such state and the overcompleteness of coherent states, i.e., $\langle\beta|\alpha\rangle \neq \delta_{\alpha,\beta}$, it is possible to generate a pseudothermal state by choosing suitable phase and intensity modulations according to a specific weighing distribution known as the Gluber-Sudarshan P representation [44]. Referencing Fig. 2, two $LiNbO_3$ modulators, the phase modulator (PM) and the amplitude modulator (AM), were chosen to provide both phase and amplitude modulations to the coherent states generated by the VCSEL. The AM was a Mach-Zehnder type of modulator including two electrical inputs: one for the controlling dc bias and one for the modulating rf signal. The PM included only an rf input used to induce a change to the transmission velocity of a laser pulse as it traveled through the inscribed waveguide. Both modulators were isolated both thermally and mechanically to limit interference and enhance operational stability. The rf signals for each unit were chosen so that the AM would apply a Gaussian modulation according to the thermal state P function and the PM would apply a random-phase change over the entire complex plane $[0, 2\pi)$ ensuring that the phase randomness would not skew the distribution [70]. The degree of "thermality" of the states produced was tested at the tomography stage by means of a HBT type of experiment to estimate the autocorrelation function $g^{(2)}(\tau)$. We used the Qucoa analysis software for real-time estimation together with the HydraHarp 400 (PicoQuant) TCSPC module. Figure 6 shows the computed $g^{(2)}(\tau)$ as a function of the time delay between detectors D_A and D_B for a pulsed source with a repetition rate of 1 MHz. The results showed a maximum at zero delay of $g^{(2)}(0) = 1.879 \pm 0.005$, in close agreement with the theoretical value of a true thermal source.

APPENDIX D: INTERFEROMETRIC CALIBRATION AND TUNING

The experimental setup of Fig. 2 can be simplified to two interwoven interferometers: the inner one [dubbed displacement interferometer (DI)] includes the optical paths connecting BS_1 to BS_3 and the outer interferometer

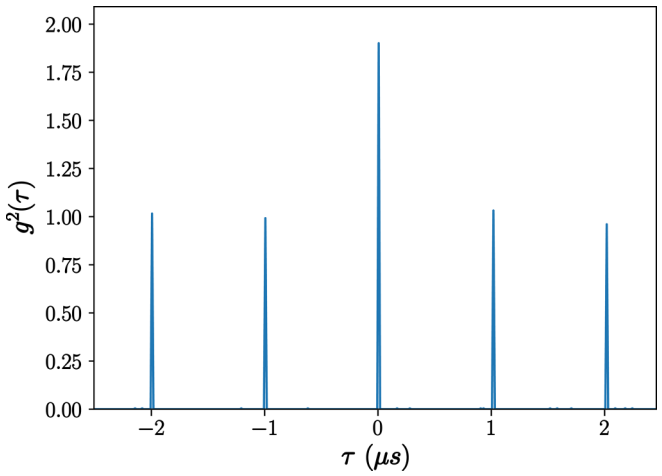

FIG. 6. Estimation of the autocorrelation function $g^{(2)}(\tau)$ of the pseudothermal state in a pulsed configuration. The function reaches a maximum value of $g^{(2)}(0) = 1.879$ at zero delay which is consistent with the expected value for a true thermal source.

constitutes the tomography stage (TS) with BS_T. As the name implies, the displacement interferometer operates the GD operation on the thermal state via the coherent state $|\beta\rangle\langle\beta|$ while the tomography stage is used to retrieve the phase and intensity information of the displaced thermal state via coherent-state routing. Multiplexed reference signals were used to tune and calibrate each interferometer independently in order to achieve optimal visibility and stability throughout the experiment. The reference signals used for DI were two bright coherent states with a phase difference of π interfering constructively and destructively at BS_3 whose output was monitored by detector D_0. Using an in-house MATLAB script, real-time visibility estimation was performed and a feedback loop mechanism provided the ability to change the relative phase difference between the pulses via the adjustable air gap connected to BS_3. Similarly, TS underwent the same calibration procedure; however, only one reference signal was used to evaluate the system's interferometric visibility since both output modes of BS_T were actively monitored by two detectors, i.e., for a given phase difference between the two input modes, either D_A or D_B saw constructive or destructive interference while the other saw destructive or constructive interference. Throughout the acquisition time, interferometric visibilities were kept constant at 98 and 97% for DI and TS, respectively, ensuring optimal temporal and spatial overlap of the different states at BS_3 and BS_T.

[1] T. B. Pittman, Y. H. Shih, D. V. Strekalov, and A. V. Sergienko, Optical imaging by means of two-photon quantum entanglement, Phys. Rev. A **52**, R3429 (1995).

[2] A. Gatti, E. Brambilla, and L. A. Lugiato, Entangled Imaging and Wave-Particle Duality: From the Microscopic to the Macroscopic Realm, Phys. Rev. Lett. **90**, 133603 (2003).

[3] J. Hance and J. Rarity, Counterfactual ghost imaging, npj Quantum Information **7**, 1 (2020).

[4] R. S. Aspden, N. R. Gemmell, P. A. Morris, D. S. Tasca, L. Mertens, M. G. Tanner, R. A. Kirkwood, A. Ruggeri, A. Tosi, R. W. Boyd, G. S. Buller, R. H. Hadfield, and M. J. Padgett, Photon-sparse microscopy: visible light imaging using infrared illumination, Optica **2**, 1049 (2015).

[5] D. V. Strekalov, A. V. Sergienko, D. N. Klyshko, and Y. H. Shih, Observation of Two-Photon "Ghost" Interference and Diffraction, Phys. Rev. Lett. **74**, 3600 (1995).

[6] A. F. Abouraddy, B. E. A. Saleh, A. V. Sergienko, and M. C. Teich, Role of Entanglement in Two-Photon Imaging, Phys. Rev. Lett. **87**, 123602 (2001).

[7] X. Yao, X. Liu, L. You, Z. Wang, X. Feng, F. Liu, K. Cui, Y. Huang, and W. Zhang, Quantum secure ghost imaging, Phys. Rev. A **98**, 063816 (2018).

[8] R. S. Bennink, S. J. Bentley, and R. W. Boyd, Two-Photon Coincidence Imaging with a Classical Source, Phys. Rev. Lett. **89**, 113601 (2002).

[9] A. Gatti, E. Brambilla, M. Bache, and L. A. Lugiato, Ghost Imaging with Thermal Light: Comparing Entanglement and Classical Correlation, Phys. Rev. Lett. **93**, 093602 (2004).

[10] M. N. O'Sullivan, K. W. C. Chan, and R. W. Boyd, Comparison of the signal-to-noise characteristics of quantum versus thermal ghost imaging, Phys. Rev. A **82**, 053803 (2010).

[11] M. J. Padgett and R. W. Boyd, An introduction to ghost imaging: Quantum and classical, Phil. Trans. R. Soc. A **375**, 20160233 (2017).

[12] J. H. Shapiro and R. W. Boyd, The physics of ghost imaging, Quant. Info. Proc. **11**, 949 (2012).

[13] M. C. Teich and B. E. Saleh, I Photon bunching and antibunching, Prog. Opt. **26**, 1 (1988).

[14] B. L. Morgan and L. Mandel, Measurement of Photon Bunching in a Thermal Light Beam, Phys. Rev. Lett. **16**, 1012 (1966).

[15] R. Loudon, Photon bunching and antibunching, Phys. Bull. **27**, 21 (1976).

[16] P. Marek and R. Filip, Coherent-state phase concentration by quantum probabilistic amplification, Phys. Rev. A **81**, 022302 (2010).

[17] E. Eleftheriadou, S. M. Barnett, and J. Jeffers, Quantum Optical State Comparison Amplifier, Phys. Rev. Lett. **111**, 213601 (2013).

[18] R. J. Donaldson, R. J. Collins, E. Eleftheriadou, S. M. Barnett, J. Jeffers, and G. S. Buller, Experimental Implementation of a Quantum Optical State Comparison Amplifier, Phys. Rev. Lett. **114**, 120505 (2015).

[19] R. J. Donaldson, L. Mazzarella, U. Zanforlin, R. J. Collins, J. Jeffers, and G. S. Buller, Quantum state correction using a measurement-based feedforward mechanism, Phys. Rev. A **100**, 023840 (2019).

[20] D. W. Canning, R. J. Donaldson, S. Mukherjee, R. J. Collins, L. Mazzarella, U. Zanforlin, J. Jeffers, R. R. Thomson, and G. S. Buller, On-chip implementation of the probabilistic quantum optical state comparison amplifier, Opt. Express **27**, 31713 (2019).

[21] G. Tatsi, D. W. Canning, U. Zanforlin, L. Mazzarella, J. Jeffers, and G. S. Buller, Manipulating thermal light via

displaced-photon subtraction, Phys. Rev. A **105**, 053701 (2022).
[22] V. C. Usenko and R. Filip, Feasibility of continuous-variable quantum key distribution with noisy coherent states, Phys. Rev. A **81**, 022318 (2010).
[23] C. Weedbrook, S. Pirandola, S. Lloyd, and T. C. Ralph, Quantum Cryptography Approaching the Classical Limit, Phys. Rev. Lett. **105**, 110501 (2010).
[24] C. H. Bennett, Quantum Cryptography Using Any Two Nonorthogonal States, Phys. Rev. Lett. **68**, 3121 (1992).
[25] Y. Zhao, B. Qi, X. Ma, H. K. Lo, and L. Qian, Experimental Quantum Key Distribution with Decoy States, Phys. Rev. Lett. **96**, 070502 (2006).
[26] C. C. W. Lim, M. Curty, N. Walenta, F. Xu, and H. Zbinden, Concise security bounds for practical decoy-state quantum key distribution, Phys. Rev. A **89**, 022307 (2014).
[27] C. Weedbrook, S. Pirandola, R. García-Patrón, N. J. Cerf, T. C. Ralph, J. H. Shapiro, and S. Lloyd, Gaussian quantum information, Rev. Mod. Phys. **84**, 621 (2012).
[28] S. Braunstein and P. van Loock, Quantum information with continuous variables, Rev. Mod. Phys. **77**, 513 (2005).
[29] T. Honjo, K. Inoue, and H. Takahashi, Differential-phase-shift quantum key distribution experiment with a planar light-wave circuit Mach-Zehnder interferometer, Opt. Lett. **29**, 2797 (2004).
[30] C. H. Bennett and G. Brassard, Quantum cryptography: Public key distribution and coin tossing, *Proceedings of International Conference on Computers, Systems and Signal Processing* (IEEE, New York, 1984), Vol. 175, pp. 7–11.
[31] D. Stucki, N. Brunner, N. Gisin, V. Scarani, and H. Zbinden, Fast and simple one-way quantum key distribution, Appl. Phys. Lett. **87**, 194108 (2005).
[32] F. Laudenbach, C. Pacher, C.-H. F. Fung, A. Poppe, M. Peev, B. Schrenk, M. Hentschel, P. Walther, and H. Hübel, Continuous-variable quantum key distribution with gaussian modulation-the theory of practical implementations, Adv. Quantum Technol. **1**, 1800011 (2018).
[33] F. Grosshans, G. Van Asschet, J. Wenger, R. Brouri, N. J. Cerf, and P. Grangier, Quantum key distribution using gaussian-modulated coherent states, Nature (London) **421**, 238 (2003).
[34] C. Weedbrook, S. Pirandola, and T. C. Ralph, Continuous-variable quantum key distribution using thermal states, Phys. Rev. A **86**, 022318 (2012).
[35] E. Newton, A. Ghesquière, F. L. Wilson, B. T. H. Varcoe, and M. Moseley, Quantum secrecy in thermal states, J. Phys. B: At., Mol. Opt. Phys. **52**, 125501 (2019).
[36] E. Newton, A. Ghesquière, F. L. Wilson, R. F. Guiazon, B. T. Varcoe, and M. Moseley, Quantum secrecy in thermal states II, J. Phys. B **53**, 205502 (2020).
[37] A. O. C. Davis, M. Walschaers, V. Parigi, and N. Treps, Conditional preparation of non-gaussian quantum optical states by mesoscopic measurement, New J. Phys. **23**, 063039 (2021).
[38] C. Li, L. Qian, and H.-K. Lo, Simple security proofs for continuous variable quantum key distribution with intensity fluctuating sources, npj Quantum Inf. **7**, 150 (2021).
[39] R. Goncharov, A. D. Kiselev, E. Samsonov, and V. Egorov, Continuous-variable quantum key distribution: security analysis with trusted hardware noise against general attacks, Nanosystems: Phys. Chem. Math. **13**, 372 (2022).
[40] T. Matsuura, K. Maeda, T. Sasaki, and M. Koashi, Finite-size security of continuous-variable quantum key distribution with digital signal processing, Nat. Commun. **12**, 252 (2021).
[41] J. M. Arrazola and V. Scarani, Covert Quantum Communication, Phys. Rev. Lett. **117**, 250503 (2016).
[42] B. A. Bash, A. H. Gheorghe, M. Patel, J. L. Habif, D. Goeckel, D. Towsley, and S. Guha, Quantum-secure covert communication on bosonic channels, Nat. Commun. **6**, 8626 (2015).
[43] S. Lloyd, Enhanced sensitivity of photodetection via quantum illumination, Science **321**, 1463 (2008).
[44] R. J. Glauber, The quantum theory of optical coherence, Phys. Rev. **130**, 2529 (1963).
[45] V. Scarani, H. Bechmann-Pasquinucci, N. J. Cerf, M. Dušek, N. Lütkenhaus, and M. Peev, The security of practical quantum key distribution, Rev. Mod. Phys. **81**, 1301 (2009).
[46] R. Tobin, A. Halimi, A. McCarthy, M. Laurenzis, F. Christnacher, and G. S. Buller, Three-dimensional single-photon imaging through obscurants, Opt. Express **27**, 4590 (2019).
[47] R. Tobin, A. Halimi, A. Mccarthy, X. Ren, K. J. Mcewan, S. Mclaughlin, and G. S. Buller, Long-range depth profiling of camouflaged targets using single-photon detection, Opt. Engin. **57**, 031303 (2017).
[48] K. Yoon-Ho, K. Sergei, and S. Yanhua, Quantum teleportation with a complete Bell state measurement, J. Mod. Opt. **49**, 221 (2002).
[49] J.-W. Pan, D. Bouwmeester, H. Weinfurter, and A. Zeilinger, Experimental Entanglement Swapping: Entangling Photons That Never Interacted, Phys. Rev. Lett. **80**, 3891 (1998).
[50] S. Pirandola, U. L. Andersen, L. Banchi, M. Berta, D. Bunandar, R. Colbeck, D. Englund, T. Gehring, C. Lupo, C. Ottaviani, J. L. Pereira, M. Razavi, J. Shamsul Shaari, M. Tomamichel, V. C. Usenko, G. Vallone, P. Villoresi, and P. Wallden, Advances in quantum cryptography, Adv. Opt. Photon. **12**, 1012 (2020).
[51] S. M. Barnett, G. Ferenczi, C. R. Gilson, and F. C. Speirits, Statistics of photon-subtracted and photon-added states, Phys. Rev. A **98**, 013809 (2018).
[52] G. V. Avosopiants, B. I. Bantysh, K. G. Katamadze, N. A. Bogdanova, Y. I. Bogdanov, and S. P. Kulik, Statistical parameter estimation of multimode multiphoton-subtracted thermal states of light, Phys. Rev. A **104**, 013710 (2021).
[53] F. S. Roux, Toolbox for non-classical state calculations, J. Opt. **23**, 125201 (2021).
[54] K. G. Katamadze, G. V. Avosopiants, N. A. Bogdanova, Y. I. Bogdanov, and S. P. Kulik, Multimode thermal states with multiphoton subtraction: Study of the photon-number distribution in the selected subsystem, Phys. Rev. A **101**, 013811 (2020).
[55] V. Josse, M. Sabuncu, N. J. Cerf, G. Leuchs, and U. L. Andersen, Universal Optical Amplification without Nonlinearity, Phys. Rev. Lett. **96**, 163602 (2006).
[56] C. Laflamme and A. A. Clerk, Quantum-limited amplification with a nonlinear cavity detector, Phys. Rev. A **83**, 033803 (2011).
[57] T. B. Propp and S. J. van Enk, On nonlinear amplification: improved quantum limits for photon counting, Opt. Express **27**, 23454 (2019).

[58] N. Basov, R. Ambartsumyan, V. Zuev, P. Kryukov, and V. Letokhov, Nonlinear amplification of light pulses, Sov. Phys. JETP **23**, 16 (1966).

[59] U. Zanforlin, G. Tatsi, J. Jeffers, and G. S. Buller, Dataset for "Covert information sharing via ghost displacement", Heriot-Watt University, https://doi.org/10.17861/9a38ac37-041f-4de6-ba1d-c34502a5b71b (2022).

[60] G. S. Ranganath, Black-body radiation, Resonance **13**, 115 (2008).

[61] C. Gerry, P. Knight, and P. L. Knight, *Introductory Quantum Optics* (Cambridge University, New York, 2005).

[62] R. Loudon, *The Quantum Theory of Light*, 3rd ed. (Oxford University, New York, 2000).

[63] R. H. Brown and R. Q. Twiss, A test of a new type of stellar interferometer on Sirius, Nature (London) **178**, 1046 (1956).

[64] G. Wu, D. Kuebel, and T. D. Visser, Generalized Hanbury Brown-Twiss effect in partially coherent electromagnetic beams, Phys. Rev. A **99**, 033846 (2019).

[65] M. Fox, *Quantum Optics: An Introduction*, 1st ed., Oxford Master Series in Physics (Oxford University, New York, 2006).

[66] I. D. Ivanovic, How to differentiate between non-orthogonal states, Phys. Lett. A **123**, 257 (1987).

[67] A. Chefles, E. Andersson, and I. Jex, Unambiguous comparison of the states of multiple quantum systems, J. Phys. A: Math. Gen. **37**, 7315 (2004).

[68] D. S. Mehta, K. Saxena, S. K. Dubey, and C. Shakher, Coherence characteristics of light-emitting diodes, J. Lumin. **130**, 96 (2010).

[69] M. D. Vidrighin, O. Dahlsten, M. Barbieri, M. S. Kim, V. Vedral, and I. A. Walmsley, Photonic Maxwell's Demon, Phys. Rev. Lett. **116**, 050401 (2016).

[70] U. Zanforlin, R. J. Donaldson, R. J. Collins, and G. S. Buller, Analysis of the effects of imperfections in an optical heterodyne quantum random-number generator, Phys. Rev. A **99**, 052305 (2019).